



OPEN

# Improved extraction efficiency of CsPbBr<sub>3</sub> perovskite light-emitting diodes due to anodic aluminum oxide nanopore structure

Lung-Chien Chen<sup>✉</sup> & Chien-Hong Kao

In this work, we investigate the improvement in the performance of a CsPbBr<sub>3</sub> perovskite light-emitting diode (PeLED) due to an anodic aluminum oxide (AAO) nanopore structure. The AAO structure in the CsPbBr<sub>3</sub> PeLED structure can improve the light extraction efficiency of CsPbBr<sub>3</sub> PeLEDs in two ways: the emission light in the side direction being redirected to the normal direction due to the light scattering effect caused by aluminum oxide nanopores and the effective emission area as a result of the rough surface of the AAO structure. The peak luminance, current efficiency, and external quantum efficiency (EQE) were 11,460 cd/m<sup>2</sup>, 2.03 cd/A, and 0.69% at a bias of 6.0 V, respectively. For comparison, the luminance, current efficiency, and EQE values of CsPbBr<sub>3</sub> PeLEDs with the AAO structure using 50 V of pore-expanding voltage demonstrated improvements of 282%, 190%, and 1280%, respectively, over CsPbBr<sub>3</sub> PeLEDs without the AAO structure.

Metal halide perovskites can be prepared from solution in an easy and costly method. They exhibit better thermal and chemical stability, improved luminescent color saturation, high photoluminescence quantum yields (PLQYs), narrow full width at half maximum (FWHM), and good spectral tunability, so they have received significant attention. To improve the brightness and stability of perovskite light-emitting diodes (PeLEDs) so that they can achieve practical purposes, a common method is to add additives or ligands to modify the interface or surface in the PeLED structure to reduce surface defects<sup>1–10</sup>.

Anodic aluminum oxide (AAO) templates have been applied in LED structures to improve the light extraction efficiency by increasing the emitting area of LEDs<sup>11–13</sup>. In 2017, Demchyshyn's team used nanoporous silicon and aluminum oxide films as templates. By reducing the pore size, it was found that the photoluminescence (PL) had a significant blue-shift, making the infrared shift to red. In addition to limiting the particle size to adjust the emission wavelength, confinement of perovskite nanocrystals in porous alumina films can significantly improve photoluminescence stability because alumina templates can be used for encapsulation. The results show that the turn-on voltage of the LED is approximately 2.5 V, with a current efficiency of 0.09 cd/A and an external quantum efficiency of 0.03%, while the PLQY of perovskite nanowires can be as high as 90%<sup>14</sup>. In 2020, Lin et al. used a combination of inkjet printing and nanoporous anodic aluminum oxide (AAO) for lasers and wide color gamut phosphors to fabricate printed perovskite nanowires (NWs). Due to the presence of AAO templates, the compact space confinement within and the perovskite encapsulation process combined with a highly stable emission intensity. It was only 19% lower after 250 h of continuous excitation with 30 mW/cm<sup>2</sup> UV and only 30% lower after storage for 3 months in 50% humidity air<sup>15</sup>. In 2017, Waleed's team synthesized nanowires (NWs) in anodized aluminum oxide films by a chemical vapor deposition (CVD) method. The results showed that the small size of anodized aluminum oxide increased the surface area of perovskite, and the high surface energy contributed to stabilizing the cubic phase. Additionally, anodized aluminum oxide protects against the invasion of water and oxygen molecules, which can significantly improve the lifetime of perovskites<sup>16</sup>. Therefore, in this work, we studied the characteristics of CsPbBr<sub>3</sub> perovskite light-emitting diodes with anodic aluminum oxide nanopore structures.

Department of Electro-Optical Engineering, National Taipei University of Technology, Taipei 10608, Taiwan. ✉email: ocean@ntut.edu.tw

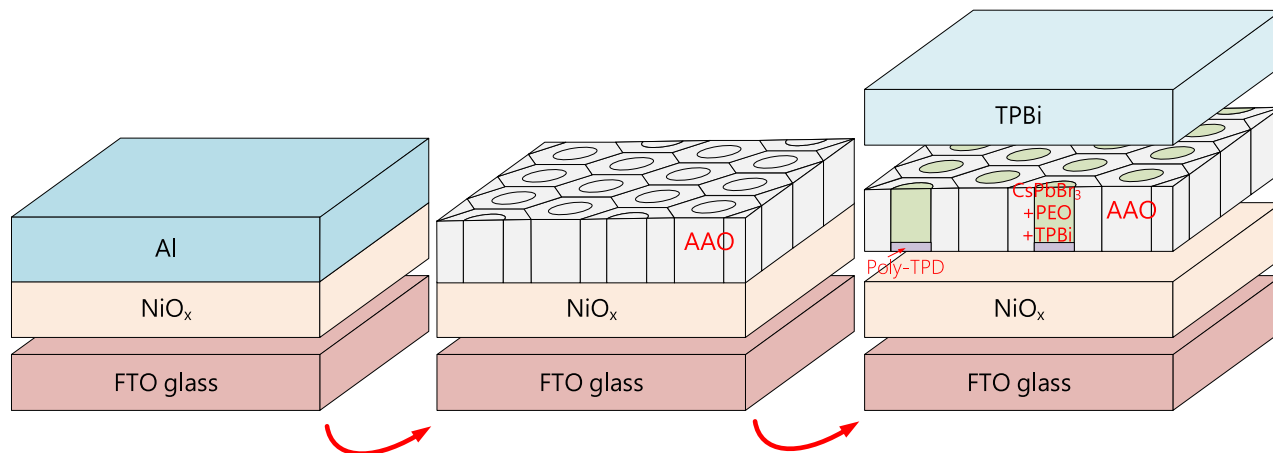


**Figure 1.** Schematic diagram of the device process flow.

## Experimental procedure

**Materials and precursors.**  $\text{NiO}_x$  powder (0.923 g) was added to 10 mL of ethylene glycol, 0.67 mL of ethylenediamine, and 0.60 mL of ethanolamine and then stirred at 500 rpm overnight to obtain a  $\text{NiO}_x$  solution. PEO powder (0.01 g) was added to 1 mL DMSO and then stirred at 700 rpm at 70 °C for 60 min to obtain a polyethylene oxide (PEO) solution.  $\text{CsBr}$  powder (0.0958 g) and  $\text{PbBr}_2$  powder (0.1101 g) were added to 1 mL of DMSO solution and then stirred at 750 rpm at 140 °C for 30 min to obtain a  $\text{CsPbBr}_3$  solution. Next, the  $\text{CsPbBr}_3$  solution was mixed with 0.4 mL PEO solution and 1 mg TPBi powder and then stirred at 750 rpm overnight to prepare the  $\text{CsPbBr}_3:(\text{PEO}, \text{TPBi})$  precursor.

**Device fabrication.** The FTO glass substrates were washed using acetone and ethanol for 10 min each and UV ozone treatment for 15 min, sequentially, to remove organic impurities and moisture. The 30-nm-thick  $\text{NiO}_x$  layer as a hole injection layer was spin-coated on FTO glass substrates at 4500 rpm for 90 s and annealed in air at 350 °C for 10 min. The 200-nm-thick Al film was evaporated on FTO/ $\text{NiO}_x$  substrates. Next, the AAO process was carried out by using oxalic acid (0.3 M) as the electrolytic solution, FTO/ $\text{NiO}_x$ /Al as the anode, and a carbon rod as the cathode, and then the substrates were put into the  $\text{H}_3\text{PO}_4$  solution for 12 min to expand the pores to form an AAO template with through-pores. Sequentially, the FTO/ $\text{NiO}_x$ /AAO template substrate was transferred into a  $\text{N}_2$ -filled glove box.

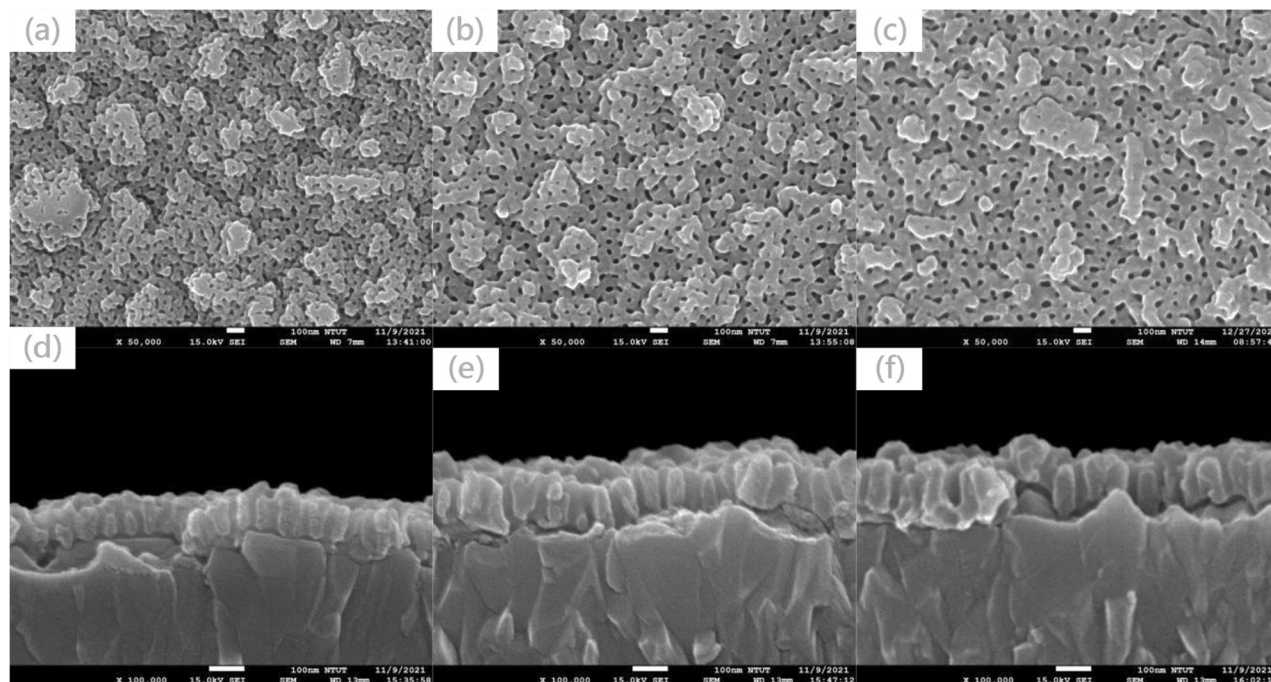
The poly-TPD solution was spin-coated on the FTO/ $\text{NiO}_x$ /AAO template substrates at 4000 rpm for 60 s and annealed at 100 °C for 10 min to form the hole transport layer. The perovskite  $\text{CsPbBr}_3:(\text{PEO}, \text{TPBi})$  blend solution was spin-coated at 3000 rpm for 60 s and annealed at 80 °C for 10 min to form an FTO/ $\text{NiO}_x$ /poly-TPD/ $\text{CsPbBr}_3:(\text{PEO}, \text{TPBi})$  structure with a 150-nm-thick active layer. Finally, a 10-nm-thick TPBi electron transport layer and 100-nm-thick Ag cathode were sequentially deposited by a thermal coater to complete the  $\text{CsPbBr}_3$  PeLED with an AAO structure. The active area of the  $\text{CsPbBr}_3$  PeLEDs with an AAO structure was determined to be 4 mm<sup>2</sup>. Figure 1 illustrates the schematic diagram of the device process flow.

**Characterization.** The characteristics of the materials and devices in this work were measured by a PANalytical X'Pert PRO MRD diffractometer (Almelo, The Netherlands) for phase identification, a Hitachi F-7000 fluorescence spectrophotometer (Tokyo, Japan) for the optical properties, a ZEISS Sigma field emission scanning electron microscope (FESEM) (Munich, Germany) for the top view and cross-sectional images, and a Photo Research spectroradiometer PR-670 (Syracuse, NY, USA) for the optoelectronic parameters PeLEDs.

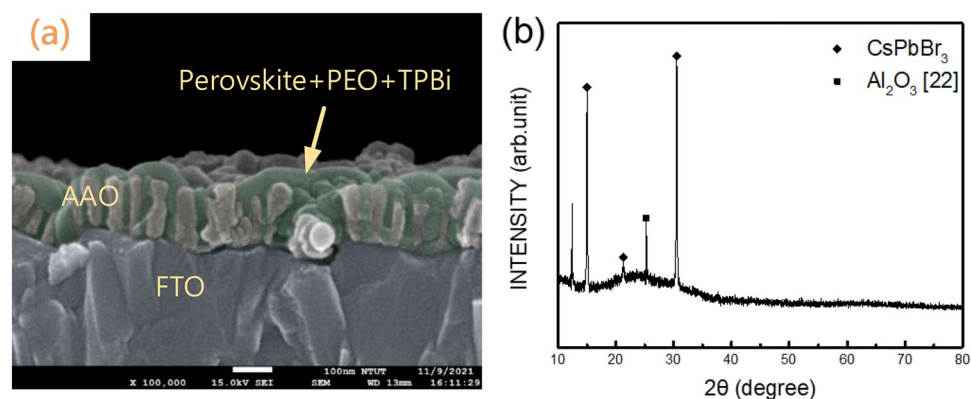
## Results and discussion

To allow the  $\text{CsPbBr}_3$  perovskite solution to flow into the pores of AAO, after the AAO film was completed, the pores were expanded by  $\text{H}_3\text{PO}_4$  for 12 min. Figure 2 shows the top view and cross-sectional SEM images of AAO with various pore-expanding voltages. The average pore sizes of the AAO structures with pore-expanding voltages of 30, 40, and 50 V are 28.57, 32.14, and 37.71 nm, respectively. As the applied voltage increases, the pore size increases and most effectively removes the lower-most AAO layer so that the AAO does not block the  $\text{CsPbBr}_3$  perovskite layer from forming on top of the poly-TPD hole transport layer, thus allowing the injection current to flow through. Also, the thickness increases and to be contributive to extraction more ray from PeLED inside<sup>17</sup>.

Figure 3a shows the cross-sectional SEM image of the  $\text{CsPbBr}_3$  perovskite/AAO structure. Observably, the  $\text{CsPbBr}_3$  perovskite film covered and penetrated the AAO film. Figure 3b plots the XRD pattern of the  $\text{CsPbBr}_3$  perovskite film coated onto and into the AAO film. In terms of XRD analysis, as shown in Fig. 3b, the XRD characteristic peaks of perovskite  $\text{CsPbBr}_3$  are approximately 15°, 21°, 31.1°, corresponding to the (101), (121), and (202) phases of the cubic lattice structure, respectively<sup>18–20</sup>. Additionally, there is a clear peak at approximately  $2\theta = 13.1^\circ$ , which corresponds to the lattice plane of (101), presumably because it is produced by the protruding orthorhombic planes of perovskites<sup>21</sup>.



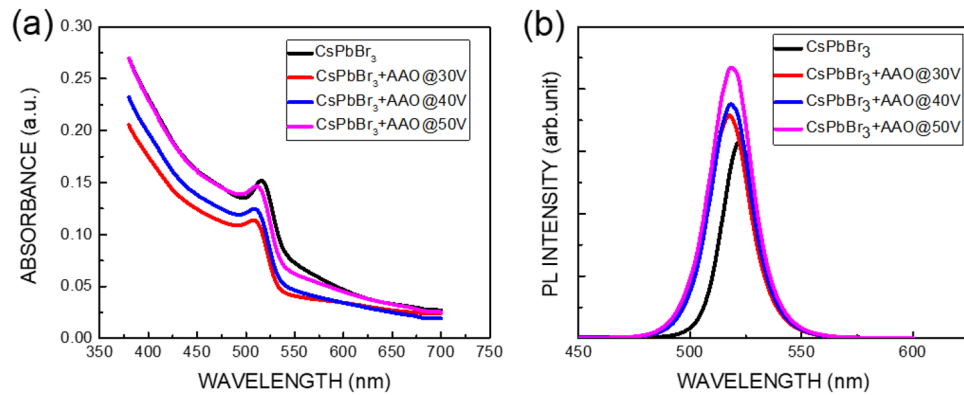
**Figure 2.** Top view and cross-sectional SEM images of AAO with various pore-expanding voltages: (a,d): 30 V, (b,e): 40 V; and (c,f): 50 V.



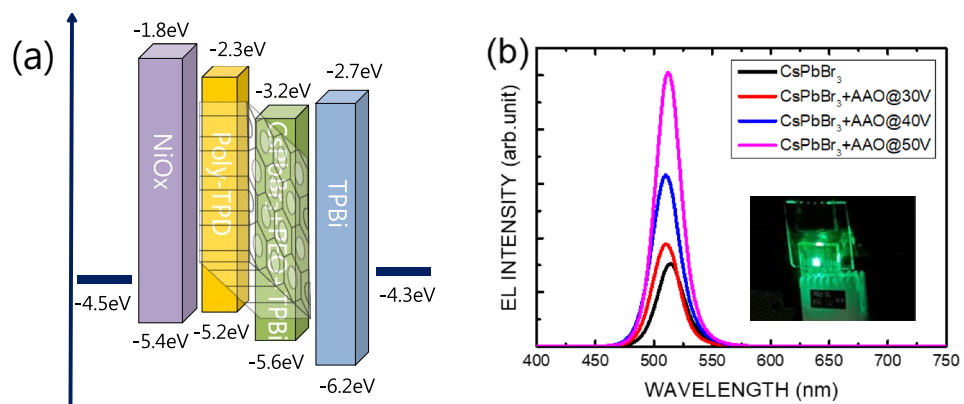
**Figure 3.** (a) Cross-sectional SEM image and (b) XRD pattern of the CsPbBr<sub>3</sub> perovskite film coated onto and into AAO films.

Figure 4 plots the absorbance and photoluminescence (PL) spectra of the CsPbBr<sub>3</sub> perovskite film on and in AAO films. The absorption edges of the CsPbBr<sub>3</sub> perovskite film with and without AAO films are 510 nm (2.431 eV) and 514 nm (2.412 eV), respectively, and the peaks of the PL spectrum of the CsPbBr<sub>3</sub> perovskite film with and without AAO films are 518 nm (2.394 eV) and 522 nm (2.375 eV), respectively. The blue-shift of approximately 8 nm between the absorbance and PL spectra for the CsPbBr<sub>3</sub> perovskite film with and without AAO films may be due to the Stoke shift<sup>22,23</sup>. The energy shift between absorbance and PL spectra is 37 meV, corresponding to the  $\frac{3}{2}kT$ , where  $k$  is Boltzmann constant, and  $T$  is temperature). Therefore, the Stoke shift of 8 nm is caused by the thermal energy from the excitation laser. The blue-shift of approximately 4 nm for the CsPbBr<sub>3</sub> perovskite film with and without AAO films may be caused by the pore size effect caused by the bandgap modulation<sup>23–25</sup>.

Figure 5a sketches the diagram of the electron level of the CsPbBr<sub>3</sub> PeLED in this work. Figure 5b plots the electroluminescence (EL) spectra of the CsPbBr<sub>3</sub> PeLEDs with and without the AAO structure for various pore-expanding voltages. The inset of Fig. 5b is a photo of the CsPbBr<sub>3</sub> PeLED with an AAO structure and a pore-expanding voltage of 50 V operating at a bias of 6 V. The peak position of the EL spectrum of the CsPbBr<sub>3</sub> PeLED without an AAO structure is 514 nm. The peak position of the EL spectrum of CsPbBr<sub>3</sub> PeLEDs with an AAO structure with 30 and 40 V of pore-expanding voltages is 510 nm. The peak position of the EL spectrum of the CsPbBr<sub>3</sub> PeLED with an AAO structure with a 50 V pore-expanding voltage is 512 nm. The blue-shift



**Figure 4.** (a) Absorbance and (b) photoluminescence (PL) spectra of CsPbBr<sub>3</sub> perovskite film on and in AAO films.



**Figure 5.** (a) Diagram of the electron level of a CsPbBr<sub>3</sub> PeLED with AAO. (b) Electroluminescence (EL) spectra of the CsPbBr<sub>3</sub> PeLEDs with and without AAO structures for various pore-expanding voltages. The inset of (b) is a photo of the CsPbBr<sub>3</sub> PeLED with an AAO structure and a pore-expanding voltage of 50 V.

is consistent with the results of the PL spectra. The blue-shift of approximately 2–4 nm between the CsPbBr<sub>3</sub> perovskite film with and without AAO structure may be caused by the pore size effect owing to the size issue of the CsPbBr<sub>3</sub> perovskite nanowires in AAO structure and CsPbBr<sub>3</sub> perovskite film status<sup>24–26</sup>.

Figures 6a–d show the current density, luminance, current efficiency, and external quantum efficiency (EQE) of CsPbBr<sub>3</sub> perovskite LEDs (PeLEDs) with and without an AAO structure. As shown in Fig. 6a, when the AAO structure was applied to the CsPbBr<sub>3</sub> PeLED structure, the turn-on voltage of the PeLEDs increased from 3 to 4 V due to a reduction in the contact area between the NiO hole injection layer and the poly-TPD hole transport layer. The luminance, current efficiency, and EQE of CsPbBr<sub>3</sub> PeLEDs without an AAO structure are approximately 3000 cd/m<sup>2</sup>, 0.1 cd/A, and 0.05%, respectively at bias of 6 V. The luminance of CsPbBr<sub>3</sub> PeLEDs with an AAO structure was superior to that of CsPbBr<sub>3</sub> PeLEDs without an AAO structure, even if the turn-on voltage increased owing to the reduction in contact area. As shown in Fig. 6b–d, the luminance of CsPbBr<sub>3</sub> PeLEDs with the AAO structure and pore-expanding voltages of 30, 40, and 50 V were approximately 4000, 6000, and 10,000 cd/m<sup>2</sup>, respectively, at bias of 6 V. The current efficiency of CsPbBr<sub>3</sub> PeLEDs with an AAO structure and pore-expanding voltages of 30, 40, and 50 V was approximately 0.5, 0.4, and 2 cd/A, respectively. The EQE of CsPbBr<sub>3</sub> PeLEDs with AAO structures and pore-expanding voltages of 30, 40, and 50 V was approximately 0.1, 0.2, and 0.7%, respectively. The peak luminance, current efficiency, and EQE were 11,460 cd/m<sup>2</sup>, 2.03 cd/A, and 0.69% at a bias of 6.0 V, respectively. Compared to the performance of CsPbBr<sub>3</sub> PeLEDs without AAO structures, the peak luminance, current efficiency, and EQE values of CsPbBr<sub>3</sub> PeLEDs with an AAO structure using a 50 V pore-expanding voltage demonstrated improvements of 282%, 190%, and 1280%, respectively. There are several high performance PeLEDs have published by employed advanced structure to boost the luminance of PeLEDs<sup>27–29</sup>. In this work, the improvement of performance is the scattering owing to the increased surface area of perovskite caused by AAO structure because the shape of AAO structure is rough, according to the SEM images in Figs. 2 and 3. Besides, a larger emission area caused by the random shape of AAO structure also means a larger injection area and to emit more photons as more charges are injected. The EQE of PeLEDs is product of the light output coupling efficiency and internal quantum efficiency (IQE)<sup>30</sup>. Therefore, the improvement of EQE in this work may be attributed to the light output coupling efficiency caused by the scattering of surface and IQE caused by the carrier recombination inside AAO structure. Figure 7 plots the emission diagram of the

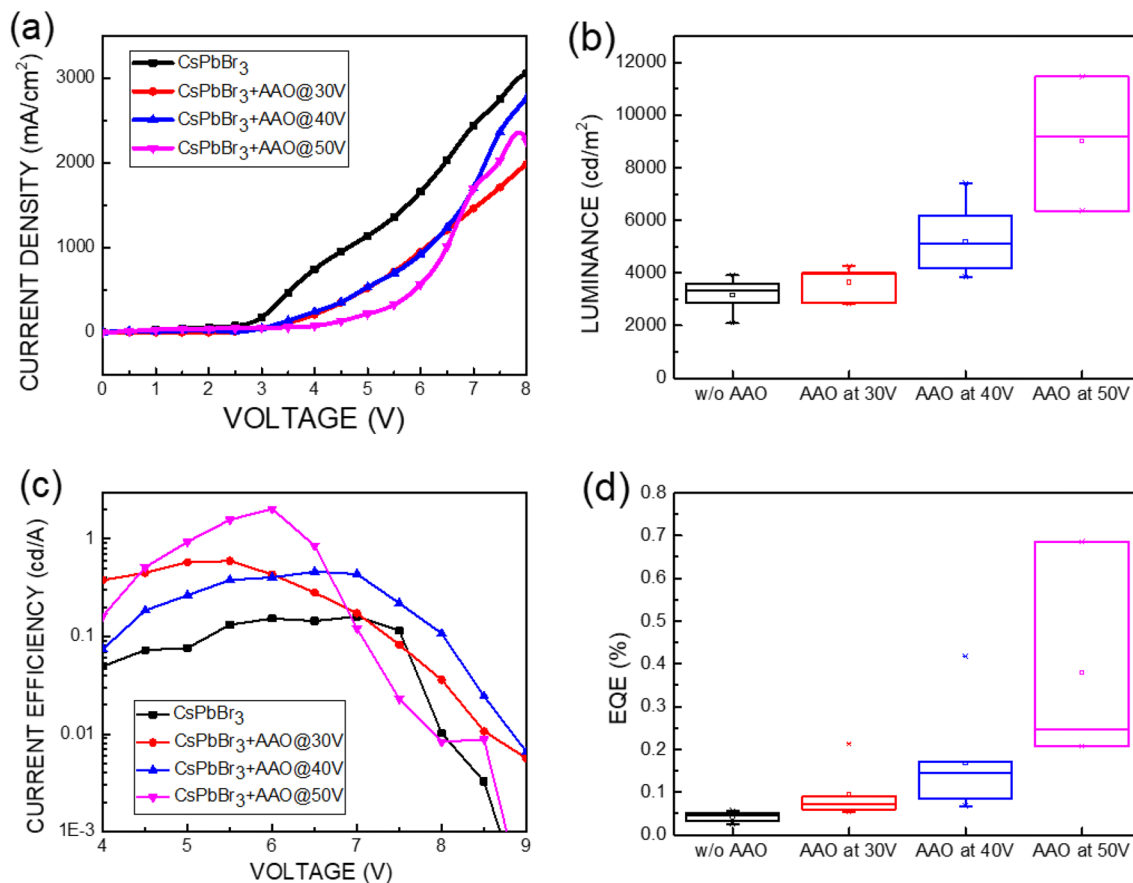


**Figure 6.** (a) Current density, (b) luminance, (c) current efficiency, and (d) external quantum efficiency (EQE) of CsPbBr<sub>3</sub> perovskite LEDs with and without AAO structures.

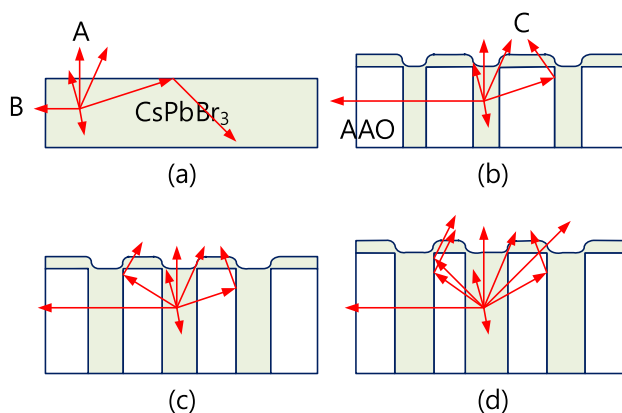


**Figure 7.** Emission diagram of the CsPbBr<sub>3</sub> active layer without and with the AAO structure using expanded pore treatment: (a) without the AAO structure, (b) with the AAO structure using 30 V treatment, (c) with the AAO structure using 40 V treatment, and (d) with the AAO structure using 50 V treatment.

CsPbBr<sub>3</sub> active layer without and with the AAO structure using a pore-expanding voltage treatment. The thicknesses of the AAO structures with pore-expanding voltages of 30, 40, and 50 V are approximately 100, 140, and 160 nm, respectively, as shown in Fig. 2d–f. As shown in Fig. 7a, the thickness of the CsPbBr<sub>3</sub> film formed by spin coating is approximately 95 nm. When using a spectrometer to measure the luminous intensity of an LED, only light in the normal direction (ray A) will be detected by the detector of the spectrometer, and light in the side direction (ray B) will not be detected. The AAO structure allows the light in the side direction to be directed to the normal direction (ray C), which is detected by the detector of the spectrometer. A thicker AAO structure means that more side light is directed to the normal direction, so the luminous intensity is brighter, as shown in

Fig. 7b–d. To compare the CsPbBr<sub>3</sub> PeLEDs with an EQE over 20%, the current efficiency of this work is lower one order<sup>31,32</sup>. The future work of PeLED should be in capping layer and passivation of non-radiative defects.

## Conclusions

We have demonstrated the performance of CsPbBr<sub>3</sub> perovskite light-emitting diodes (PeLEDs) with AAO structures. The peak luminance, current efficiency, and EQE were 11,460 cd/m<sup>2</sup>, 2.03 cd/A, and 0.69% at a bias of 6.0 V, respectively. Compared to the performance of CsPbBr<sub>3</sub> PeLEDs without AAO structures, the peak luminance, current efficiency, and EQE values of CsPbBr<sub>3</sub> PeLEDs with an AAO structure using a 50 V pore-expanding voltage demonstrated improvements of 282%, 190%, and 1280%, respectively. The performance improvement may be attributed to two factors. One is the scattering owing to the increased surface area of perovskite caused by AAO structure because the shape of AAO structure is rough. The other factor is the increase in effective emission area as a result of the random shape of the AAO structure.

## Data availability

The datasets used and/or analyzed during the current study available from the corresponding author on reasonable request.

Received: 13 June 2022; Accepted: 24 August 2022

Published online: 30 August 2022

## References

- Kim, M., Motti, S. G., Sorrentino, R. & Petrozza, A. Enhanced solar cell stability by hygroscopic polymer passivation of metal halide perovskite thin film. *Energy Environ. Sci.* **11**, 2609–2619. <https://doi.org/10.1039/C8EE01101J> (2018).
- Zhang, H. *et al.* Efficient and stable chemical passivation on perovskite surface bidentate anchoring. *Adv. Energy Mater.* **9**, 1803573. <https://doi.org/10.1002/aenm.201803573> (2019).
- Zuo, L. J. *et al.* Polymer-modified halide perovskite films for efficient and stable planar heterojunction solar cells. *Sci. Adv.* **3**, 1700106. <https://doi.org/10.1126/sciadv.1700106> (2017).
- Jiang, Q. *et al.* Surface passivation of perovskite film for efficient solar cells. *Nat. Photon.* **13**, 460–466. <https://doi.org/10.1038/s41566-019-0398-2> (2019).
- Chen, L. C., Tien, Y. H. & Tian, J. Influence of surface passivation on perovskite CsPbBr<sub>1.2</sub>I<sub>1.8</sub> quantum dots and application of high purity red light-emitting diodes. *J. Alloys Compd.* **892**, 162140. <https://doi.org/10.1016/j.jallcom.2021.162140> (2022).
- Tian, S. *et al.* Additive and interfacial control for efficient perovskite light-emitting diodes with reduced trap densities. *J. Semicond.* **43**, 050502. <https://doi.org/10.1088/1674-4926/43/5/050502> (2022).
- Zhao, B. *et al.* Efficient light-emitting diodes from mixed-dimensional perovskites on a fluoride interface. *Nat. Electron.* **3**, 704–710. <https://doi.org/10.1038/s41928-020-00487-4> (2020).
- Liu, Y., Ono, L. K. & Qi, Y. Organic additive engineering toward efficient perovskite light-emitting diodes. *InfoMat* **2**, 1095–1108. <https://doi.org/10.1002/inf2.12098> (2020).
- Zhu, L. *et al.* Unveiling the additive-assisted oriented growth of perovskite crystallite for high performance light-emitting diodes. *Nat. Commun.* **12**, 5081. <https://doi.org/10.1038/s41467-021-25407-8> (2021).
- Zou, Y. *et al.* Boosting perovskite light-emitting diode performance via tailoring interfacial contact. *ACS Appl. Mater. Interfaces* **10**, 24320–24326. <https://doi.org/10.1021/acsami.8b07438> (2018).
- Huang, Y. R. *et al.* Light extraction efficiency enhancement of flip-chip blue light-emitting diodes by anodic aluminum oxide. *Beilstein J. Nanotechnol.* **9**, 1602–1612. <https://doi.org/10.3762/bjnano.9.152> (2018).
- Wang, C. C. *et al.* Improved extraction efficiency of light-emitting diodes by modifying surface roughness with anodic aluminum oxide film. *IEEE Photonics Technol. Lett.* **20**, 428–430. <https://doi.org/10.1109/LPT.2008.916948> (2008).
- Chen, L. C., Wang, C. K., Huang, J. B. & Hong, L. S. A nanoporous AlN layer patterned by anodic aluminum oxide and its application as a buffer layer in a GaN-based light-emitting diode. *Nanotechnology* **20**, 085303. <https://doi.org/10.1088/0957-4484/20/8/085303> (2009).
- Demchyshyn, S. *et al.* Confining metal-halide perovskites in nanoporous thin films. *Sci. Adv.* **3**, e1700738. <https://doi.org/10.1126/sciadv.1700738> (2017).
- Lin, C. H. *et al.* Designed growth and patterning of perovskite nanowires for lasing and wide color gamut phosphors with long-term stability. *Nano Energy* **73**, 104801. <https://doi.org/10.1016/j.nanoen.2020.104801> (2020).
- Waleed, A. *et al.* All inorganic cesium lead iodide perovskite nanowires with stabilized cubic phase at room temperature and nanowire array-based photodetectors. *Nano Lett.* **17**, 4951–4957. <https://doi.org/10.1021/acs.nanolett.7b02101> (2017).
- Jiang, S. *et al.* Study on light extraction from GaN-based green light-emitting diodes using anodic aluminum oxide pattern and nanoimprint lithography. *Sci. Rep.* **6**, 21573. <https://doi.org/10.1038/srep21573> (2016).
- Li, C. *et al.* Highly compact CsPbBr<sub>3</sub> perovskite thin films decorated by ZnO nanoparticles for enhanced random lasing. *Nano Energy* **40**, 195–202. <https://doi.org/10.1016/j.nanoen.2017.08.013> (2017).
- Haruta, Y., Ikenoue, T., Miyake, M. & Hirato, T. Fabrication of (101)-oriented CsPbBr<sub>3</sub> thick films with high carrier mobility using a mist deposition method. *Appl. Phys. Exp.* **12**, 085505. <https://doi.org/10.7567/1882-0786/ab2c96> (2019).
- Li, C. T., Lee, K. L., Wang, S. F. & Chen, L. C. Effect of a rubidium chloride carrier confinement layer on the characteristics of CsPbBr<sub>3</sub> perovskite light-emitting diodes. *Nanoscale Res. Lett.* **17**, 2. <https://doi.org/10.1186/s11671-021-03641-9> (2022).
- Kostopoulou, A., Sygletou, M., Brintakis, K., Lappasa, A. & Stratakis, E. Low-temperature benchtop-synthesis of all-inorganic perovskite nanowires. *Nanoscale* **9**, 18202–18207. <https://doi.org/10.1039/c7nr06404g> (2017).
- Zhang, L., Zhang, Y., He, W., Peng, H. & Dai, Q. CsPbBr<sub>3</sub> perovskite nanowires and their optical properties. *Opt. Mater.* **109**, 110399. <https://doi.org/10.1016/j.optmat.2020.110399> (2020).
- Madej, D., Prorok, R. & Wiśniewska, K. An experimental investigation of hydration mechanism of the binary cementitious pastes containing MgO and Al<sub>2</sub>O<sub>3</sub> micro-powders. *J. Therm. Anal. Calorim.* **134**, 1481–1492. <https://doi.org/10.1007/s10973-018-7618-8> (2018).
- Huang, H. *et al.* A growth mechanism of strongly emitting CH<sub>3</sub>NH<sub>3</sub>PbBr<sub>3</sub> perovskite nanocrystals with a tunable bandgap. *Nat. Commun.* **8**, 996. <https://doi.org/10.1038/s41467-017-00929-2> (2017).
- Zhang, Z. *et al.* Single-crystalline perovskite nanowire arrays for stable X-ray scintillators with micrometer spatial resolution. *ACS Appl. Nano Mater.* **5**, 881–889. <https://doi.org/10.1021/acsnm.1c03575> (2022).
- Oksenberg, E. *et al.* Large lattice distortions and size-dependent bandgap modulation in epitaxial halide perovskite nanowires. *Nat. Commun.* **11**, 489. <https://doi.org/10.1038/s41467-020-14365-2> (2020).

27. Chen, Z. *et al.* Utilization of trapped optical modes for white perovskite light-emitting diodes with efficiency over 12%. *Joule* **5**, 456–466. <https://doi.org/10.1016/j.joule.2020.12.008> (2021).
28. Zhang, Q. *et al.* Light out-coupling management in perovskite LEDs—What can we learn from the past?. *Adv. Funct. Mater.* **30**, 2002570. <https://doi.org/10.1002/adfm.202002570> (2020).
29. Cao, Y. *et al.* Perovskite light-emitting diodes based on spontaneously formed submicrometre-scale structures. *Nature* **562**, 249–253. <https://doi.org/10.1038/s41586-018-0576-2> (2018).
30. Shi, X. B. *et al.* Optical energy losses in organic–inorganic hybrid perovskite light-emitting diodes. *Adv. Opt. Mater.* **6**, 1800667. <https://doi.org/10.1002/adom.201800667> (2018).
31. Lin, K. *et al.* Perovskite light-emitting diodes with external quantum efficiency exceeding 20 per cent. *Nature* **562**, 245–248. <https://doi.org/10.1038/s41586-018-0575-3> (2018).
32. Liu, Z. *et al.* Perovskite light-emitting diodes with EQE exceeding 28% through a synergetic dual-additive strategy for defect passivation and nanostructure regulation. *Adv. Mater.* **33**, 2103268. <https://doi.org/10.1002/adma.202103268> (2021).

## Acknowledgements

This research was supported by the Ministry of Science and Technology (Taiwan) under Contract No. 110-2221-E-027-125.

## Author contributions

L.-C.C.: Conceptualization, Methodology, Investigation, Funding acquisition, Writing—original draft, Writing—review & editing, Supervision. C.-H.K.: Methodology, Investigation, Performed measurements, Prepared the graphics. All authors approved this manuscript.

## Competing interests

The authors declare no competing interests.

## Additional information

**Correspondence** and requests for materials should be addressed to L.-C.C.

**Reprints and permissions information** is available at [www.nature.com/reprints](http://www.nature.com/reprints).

**Publisher's note** Springer Nature remains neutral with regard to jurisdictional claims in published maps and institutional affiliations.



**Open Access** This article is licensed under a Creative Commons Attribution 4.0 International License, which permits use, sharing, adaptation, distribution and reproduction in any medium or format, as long as you give appropriate credit to the original author(s) and the source, provide a link to the Creative Commons licence, and indicate if changes were made. The images or other third party material in this article are included in the article's Creative Commons licence, unless indicated otherwise in a credit line to the material. If material is not included in the article's Creative Commons licence and your intended use is not permitted by statutory regulation or exceeds the permitted use, you will need to obtain permission directly from the copyright holder. To view a copy of this licence, visit <http://creativecommons.org/licenses/by/4.0/>.

© The Author(s) 2022